A New Kinetic Representation of Fluctuation-Driven Neuronal Networks with Application to Simple & Complex Cells in Primary Visual Cortex

D. Cai[1], L. Tao[1,2,3], M. Shelley[1,2], and D. McLaughlin[1,2]

[1] Courant Institute of Mathematical Sciences
NYU, 251 Mercer Street, New York, NY 10012, and
Center for Neural Science, NYU
4 Washington Place, New York, NY 10003

[2] Department of Mathematical Sciences and
Center for Applied Mathematics and Statistics
New Jersey Institute of Technology, Newark, NJ 07102

[3] Center for Neural Science, NYU
4 Washington Place, New York, NY 10003

CAMS Report 0304-28, Spring 2004

Center for Applied Mathematics and Statistics

NJIT

A New Kinetic Representation of Fluctuation-Driven Neuronal Networks with Application to Simple & Complex Cells in Primary Visual Cortex

David Cai[†], Louis Tao[†‡*], Michael Shelley[†‡]and David W. McLaughlin[†‡]

[†] *Courant Institute of Mathematical Sciences &*
[‡] *Center for Neural Science*
New York University, New York, NY 10012
[*] *Department of Mathematical Sciences, New Jersey Institute of Technology, Newark, NJ 07102*

Abstract A new coarse-grained representation of the dynamics of neuronal networks is introduced and developed in terms of kinetic equations, which, via a novel moments *closure*, are derived mathematically, directly from the original large-scale integrate-and-fire (I&F) network. This powerful kinetic theory can capture the full dynamic range of neuronal networks — from the mean-driven limit (a limit as the number of neurons $N \to \infty$, in which the fluctuations vanish) to the *fluctuation-dominated limit* (such as in small N networks). Comparison with full numerical simulations of the original I&F network establishes that the reduced dynamics is very accurate and numerically efficient over all dynamic ranges. Both analytical insights and numerical scale-up of neuronal computation can be achieved via this kinetic approach. Here the theory is illustrated by a study of the dynamical properties of networks of various architectures, including excitatory and inhibitory neurons of both simple and complex type, which exhibit rich phenomena, e.g., transition to bistability and hysteresis, even in the presence of large fluctuations. The implication for possible connections between the structure of the bifurcations and the behavior of complex cells is discussed. Finally, I&F networks and kinetic theory are used to discuss orientation selectivity of complex cells for "ring model" architectures which characterize changes in the response of neurons located from near to far from "orientation pinwheel centers".

1 Introduction

Frequently neuronal networks, whether real cortical networks [1] or computer models [2, 3], operate in a regime in which spiking is caused by irregular temporal fluctuations of the membrane potential. At this "cortical operating point", the mean membrane potential (for example, obtained by averaging over many voltage traces under the same stimulus condition or by averaging locally in time), does not reach firing threshold. Thus, the spiking process is *fluctuation driven.*

A theoretical challenge is to construct efficient and effective representations of such fluctuation-driven networks, which are needed — both to "scale-up" computational models to large enough regions of the cortex to capture interesting cortical processing (such as optical illusions related to "contour completion"), and to gain qualitative understanding of the cortical mechanisms underlying this level of cortical processing. In this article, we present such a construction: Starting with large-scale model networks of integrate-and-fire (I&F) neurons, which are sufficiently detailed for modeling neuronal computation of large systems, but are difficult to scale-up for computation, we tile the cortex with *coarse-grained (CG) cells* — each of which is sufficiently small that the cortical architecture does not change significantly throughout the CG cell, yet sufficiently large to contain many (hundreds) of neurons. We then derive an effective dynamics to capture the behavior of the many neurons within each CG cell in the interaction with other CG cells. This representation is achieved via a kinetic theory, accomplished by a novel closure. This powerful approach allows for both computational scale-up and structural insight into the mechanisms of the cortical network. Here, we develop the method for one CG cell: (i) We benchmark the accuracy and validity of the new kinetic theory by comparing its predictions with the results of the full point-neuron simulations over all dynamic ranges, from the mean-driven limit (a limit as the number of neurons $N \to \infty$, in which the fluctuations vanish) to the *fluctuation-dominated limit* (such as in small N networks); (ii) We illustrate the power of this theory by using it to provide a qualitative intuition about mechanisms which potentially underly the behavior of simple and complex cortical cells in the primary visual cortex for macaque.

Classically, neurons in V1 are classified [4] as "simple" or "complex". Sim-

ple cells respond to visual stimulation in an essentially linear fashion — for example, responding to sinusoidally modulated standing gratings at the fundamental frequency, with the magnitude of response sensitive to the spatial phase of the grating pattern. Complex cells respond nonlinearly (with a significant second harmonic) to such temporally modulated standing gratings — with a response which is phase insensitive. It is important to note that the "simple-complex" nature of a neuron is not an individual cellular property; rather, it results from the coupling architecture of the cortical network.

In [5], we present a large-scale neuronal model in which simple and complex cells arise from the architecture of V1. In this model, a balance between cortical-cortical connections and LGN drive determines whether an individual neuron is simple or complex. (Complex cells experience strong cortical excitation, whereas simple cells are dominated by cortical inhibition.) This numerical model, while reproducing many qualitative aspects of both intracellular and extracellular measurements of simple and complex cell responses, it has yet to overcome some difficulties: (i) there are too few complex cells ($\simeq 30\%$ complex, rather than the observed 50%); (ii) Cells are not sufficiently selective for orientation. Presumably, a stronger cortical amplifier is needed; however, stronger amplification causes the numerical cortex to become unstable to synchrony, oscillations, and have too large firing rates.

Within the framework of kinetic theory, we discuss a possible resolution to these instabilities by indicating *near-bistability in fluctuation driven networks* as one possible mechanism underlying complex cell responses.

2 Methods

Our large-scale model is a detailed numerical representation of a small local patch ($1mm^2$) of input layer $4C\alpha$ of primary visual cortex (V1) of macaque monkey — constrained wherever possible by experimental measurements from anatomy, physiology, and imaging. The local patch contains 128^2 conductance based, I&F neurons — 75% excitatory and 25% inhibitory, with both simple and complex cells. The cortical architecture and the LGN drive (which sets cortical maps such as that of orientation preference with its four pinwheel centers within the local patch) are summarized in Fig. 1, and the full model is described in detail in [6, 7, 5].

The **equations of the model** have the general structure

$$\frac{dv_P^j}{dt} = -g_L \left(v_P^j - V_R\right) - g_{PE}^j(t) \left(v_P^j - V_E\right) - g_{PI}^j(t) \left(v_P^j - V_I\right), \quad P = E, I \tag{1}$$

whose evolution determines the m^{th} spike time, t_m^j, of the j^{th} model neuron, defined by $v_P^j(t_m^j -) = V_T$; $v_P^j(t_m^j + \tau_{ref}) = V_R$. Here the membrane potentials of the excitatory (E) (inhibitory (I)) neurons are denoted by v_E^j (v_I^j), where the superscript $j = (j_1, j_2)$ indexes the spatial location of the neuron within the cortical layer. We use normalized, dimensionless potentials with $V_I = -2/3, V_T = 1, V_R = 0$, and $V_E = 14/3$.

The **time-dependent conductances** arise from the input forcing (through the LGN) and from noise to the layer, as well as from the cortical network activity of the excitatory and inhibitory populations. They have the general form

$$g_{EE}^j(t) = F_{EE}(t) + [(1 - \lambda^j) S_{EE}\left(\lambda^j\right) + S_{EE}^0(\lambda^j)] \sum_k a_{j-k} \sum_l G_E(t - t_l^k),$$

where $F_{EE}(t) = \lambda^j g_{lgn}^j(t) + f_{EE}^0(t)$, and with similar expressions for $g_{EI}^j(t), g_{IE}^j$ and g_{II}^j. $S_{EE}(\lambda^j)$ denotes the synaptic strength, a_{j-k} describes the spatial decay of the coupling, and $G_E(t - t_l^k)$ the temporal time course. The conductance $f_{PE}^0(t)$ denotes random background forcing, and $g_{lgn}^j(t)$ denotes the forcing from the LGN.

The parameter $\lambda^j \in [0, 1]$ in these equations indicates heuristically how the distribution of simple and complex cells is set in the model and reflects the simple-complex nature of the j^{th} neuron (with $\lambda^j = 0$ the most complex; $\lambda^j = 1$ the most simple and S_{EE}^0 models week cortical excitatory couplings for simple cells), by setting the strength of LGN drive relative to the strength of the cortico-cortical excitation. The parameter λ^j is selected randomly for each neuron, with its distribution determining the distribution of simple and complex cells within the network [5]. (Here the general structure of the model has been summarized; for a detailed description, see [6, 7, 5].)

2.1 Sketch of Derivation of the Kinetic Theory

To reduce this large-scale numerical model, first, we partition the cortical layer with a tiling of CG cells — with each CG cell sufficiently large to

contain hundreds of neurons, yet small enough that the cortical maps and cortical architecture are roughly constant throughout that CG cell. Our goal is to develop an effective description of the dynamics of the neurons within each CG cell. This is accomplished via kinetic equations which govern the evolution of $\rho(v, g; \mathbf{x},t)$ — the probability density of finding a neuron at time t within the $\mathbf{x}^{th}$ CG cell, with voltage $v \in (v, v + dv)$ and conductance $g \in (g, g + dg)$. For computational efficiency and theoretic analysis, it is of great advantage to further reduce this kinetic theory — a $(2 + 1)$-D system in the case of single CG cell. A reduction to $(1 + 1)$-D is achieved via a moment closure.

Next, we sketch this kinetic theory and its closure reduction, for a single CG cell. Limitations of space force us to restrict our description of the derivation to a purely excitatory network containing only AMPA synapses and simple cells.

The I&F dynamics for the jth neuron in a CG cell of N excitatory neurons is

$$\tau \frac{dv^j}{dt} = -\left(v^j - V_R\right) - g^j(t)\ \left(v^j - V_E\right), \tag{2a}$$

$$\sigma \frac{dg^j}{dt} = -g^j + f \sum_l \delta(t - t_j^l) + \frac{S}{N} \sum_{l,k \neq j} \delta(t - t_k^l), \tag{2b}$$

where τ is the "leakage" time constant, σ the time constant of the AMPA synapse, f the synaptic strength from the LGN connections, t_j^l the time of the l^{th} LGN spike, t_k^l the l^{th} spike time of the k^{th} cortical neuron within the CG cell, and $\delta(\cdot)$ is the Dirac delta function. S symbolizes the cortical-cortical coupling strength. We define the probability density function (pdf) [8, 9, 10, 11, 12, 13, 14, 15, 16, 3]

$$\rho(v, g; t) \equiv \mathbb{E}[\frac{1}{N} \sum_{j=1}^{N} \left\{\delta[v - v^j(t)]\ \delta[g - g^j(t)]\right\}], \tag{3}$$

where the expectation $\mathbb{E}$ is taken over all realizations of incoming Poisson spike trains from the LGN, and over random initial conditions.

Under the assumptions that, 1) $N^{-1} \ll 1$, and 2) the summed input to a neuron from low-rate cortical spike trains (assumed to be independent) is

Poisson [17], we are able to show, from Eqs. (2), that $\rho(v,g;t)$ satisfies the following evolution equation:

$$\partial_t \rho = -\partial_v J^{(v)}(v,g;\rho) + \frac{1}{\sigma}\partial_g \ (g\rho) \\ + \nu_0(t)\left[\rho(v,g-\frac{f}{\sigma};t)-\rho(v,g;t)\right] + Nm(t)\left[\rho(v,g-\frac{S}{N\sigma};t)-\rho(v,g;t)\right], \tag{4}$$

where

$$J^{(v)}(v,g;t) = -\frac{1}{\tau}\left[(v-V_R)+g(v-V_E)\right]\rho\,(v,g,t)$$

is the flux along v, $\nu_0(t)$ is the (temporally modulated) rate for the Poisson spike train from the LGN, and $m(t)$ is the population-averaged firing rate per neuron in the CG cell, determined by the flux at the threshold:

$$m(t) = \int_0^\infty J^{(v)}(v,g;t)\Big|_{v=V_T}\, dg.$$

The discrete differences in g which appear in Eq. (4) arise from the fact that the time-course of g after an incoming spike is a single exponential (Eq. (2b)). (The theory can be readily generalized to more complicated time-courses of conductance.) For small f and large N, these differences can be approximated as derivatives, resulting in

$$\partial_t \rho = -\partial_v J^{(v)}(v,g;\rho) + \frac{1}{\sigma}\partial_g\left\{[g-\tilde{g}(t)]+\sigma_g^2\partial_g\rho\right\}; \tag{5}$$

$$\tilde{g}(t) \equiv \nu_0(t)f + m(t)S; \quad \sigma_g^2(t) \equiv \nu_0(t)\frac{f^2}{2\sigma} + m(t)\frac{S^2}{2\sigma N}. \tag{6}$$

To describe the time dynamics of conductance and voltage in fluctuation dynamics, we investigate the evolution of the marginals and conditional moments:

$$\rho^{(g)}(g;t) \equiv \int_{V_R}^{V_T} \rho(v,g;t)\ dv, \qquad \rho^{(v)}(v;t) \equiv \int_0^\infty \rho(v,g;t)\ dg, \tag{7}$$
$$\mu_n^{(v)}(v;t) \equiv \int_0^\infty g^n \rho(g|v;t)\ dg, \quad n=1,2,\cdots$$

where $\rho(g|v;t)$ is the conditional pdf, i.e., $\rho(v,g;t) = \rho(g|v;t)\ \rho^{(v)}(v;t)$.

Marginalization of Eq. (5) to v yields

$$\sigma\partial_t\rho^{(g)} = \partial_g\left\{[g-\tilde{g}(t)]\rho^{(g)} + \sigma_g^2\partial_g\rho^{(g)}\right\}, \tag{8}$$

which describes the g-fluctuations. Under vanishing boundary conditions at $g = 0$ and as $g \to \infty$, the time-invariant solution is approximated by a Gaussian. Figure 2b shows a comparison of this Gaussian approximate solution with a numerical simulation of the original I&F system. Clearly the reduced Eq. (8) accurately captures the fluctuations in g.

Integrating Eq. (5) [and g times Eq. (5)] with respect to g yields equations for the marginal $\rho^{(v)}$ [and first moment $\mu_1^{(v)}$]:

$$\partial_t\rho^{(v)} = \partial_v\left[U(v)\,\rho^{(v)}\right] \tag{9a}$$

$$\partial_t\mu_1^{(v)} = -\frac{1}{\sigma}\left(\mu_1^{(v)} - \tilde{g}(t)\right) + U(v)\,\partial_v\mu_1^{(v)} + \frac{\Sigma^2(v)}{\tau\rho^{(v)}}\partial_v\left[(v-V_E)\rho^{(v)}\right] + \frac{(v-V_E)}{\tau}\partial_v\Sigma^2(v), \tag{9b}$$

where $\Sigma^2(v) \equiv \mu_2^{(v)} - [\mu_1^{(v)}]^2$ is the conditional variance, $U(v) \equiv \tau^{-1}\left[(v-V_R) + (v-V_E)\mu\right.$

These equations are not closed because the equation for the first moment $\mu_1^{(v)}$ depends upon the second moment $\mu_2^{(v)}$. Closure is achieved through the *assumptions*

$$\partial_v\Sigma^2(v) = 0 \quad \text{and} \quad \Sigma^2(v) = \sigma_g^2,$$

yielding a closed pair of $(1+1)$-D kinetic equations for $\rho^{(v)}(v;t)$ and $\mu_1^{(v)}(v;t)$:

$$\partial_t\rho^{(v)} = \partial_v\left[U(v)\,\rho^{(v)}\right] \tag{10a}$$

$$\partial_t\mu_1^{(v)} = -\frac{1}{\sigma}\left(\mu_1^{(v)} - \tilde{g}(t)\right) + U(v)\,\partial_v\mu_1^{(v)} + \frac{\sigma_g^2}{\tau\rho^{(v)}}\,\partial_v\left[(v-V_E)\rho^{(v)}\right] \tag{10b}$$

These kinetic equations are solved for $V_R \le v \le V_T$, under two point boundary conditions in v which are derived from the fact that the flux $J^{(v)}(v,g)$ across firing threshold V_T is equal to the flux at reset V_R, adjusted for finite

refractory period. This reduction in dimension from $(2+1)$-D to $(1+1)$-D yields a significant computational savings in addition to the savings achieved by the pdf representation itself (see below).

We emphasize that this derivation extends to realistic networks containing excitatory and inhibitory neurons of both simple and complex types, with both AMPA and NMDA excitatory synapses, and with coupling between many CG cells. Results in the next section are for such realistic networks. Coupling between CG cells is accomplished by replacing Eq. (6) with

$$\tilde{g}(t;\mathbf{x}) \equiv \nu_0(t;\mathbf{x}) f + S \int a(\mathbf{x}-\mathbf{x}')\; m(t;\mathbf{x}')\; d\mathbf{x}', \tag{11a}$$

$$\sigma_g^2(t;\mathbf{x}) \equiv \nu_0(t;\mathbf{x}) \frac{f^2}{2\sigma} + \frac{S^2}{2\sigma N} \int a^2(\mathbf{x}-\mathbf{x}')\; m(t;\mathbf{x}')\; d\mathbf{x}', \tag{11b}$$

where $\mathbf{x}$ denotes the coarse-grained spatial label.

We note in passing that, as the AMPA time scale σ is much smaller than the leakage time scale τ, a further reduction can be achieved by coarse-graining in time, resulting in an effective dynamics which is useful for analytical insight. As $\sigma \to 0$, recalling that $\sigma\sigma_g^2 = \nu_0(t) f^2/2 + m(t) S^2/(2N) = O(1)$, Eq. (10b) reduces to $\mu_1^{(v)}(v;t) \simeq \tilde{g}(t) + \frac{\sigma\sigma_g^2}{\tau\rho^{(v)}} \partial_v \left[(v - V_E)\rho^{(v)}\right]$, which upon insertion into Eq. (10a) yields a closed equation for $\rho^{(v)}(v;t)$ only:

$$\tau \partial_t \rho^{(v)} = \partial_v \left\{ \left[(1+\gamma(t))\, v \;-\; [V_R + \gamma(t)\, V_E]\right] \rho^{(v)} + \frac{\sigma\sigma_g^2}{\tau} (v - V_E)^2 \partial_v \rho^{(v)} \right\}, \tag{12}$$

where $\gamma(t) = \tilde{g}(t) + \frac{\sigma\sigma_g^2}{\tau}$. We can show that this Fokker-Planck equation is consistent with a white-noise limit of the underlying stochastic processes of conductance. Notice that, as the number of neurons in the CG cell $N \to \infty$ and $f \to 0$, then $\sigma\sigma_g^2 \to 0$; thus, the fluctuations drop out of Eq. (12), and the dynamics reduces to "mean-driven" dynamics [18, 16, 2].

3 Results

Our first important result is the derivation of the reduced kinetic representation, Eqs. (10), directly from the large-scale network of I&F neurons by

the coarse-grained procedure just described. Comparing with full numerical simulations of the I&F network, this kinetic theory is surprisingly accurate, which is clearly illustrated in Fig. 2. Notice in particular the failure of mean-driven ($N \to \infty,\ f \to 0$) theory at small average input conductance G_{input} — the regime where fluctuations dominate. We point out that for physiological values of σ, had we used the diffusion limit, i.e. Eq. (12) — the $\sigma \to 0$ limit of Eq. (10), we would not be able to achieve this accuracy (see the dash-dotted line in Fig. 2).

We further illustrate the effectiveness of the kinetic dynamics in describing fluctuation-driven behavior by considering a network of only $N = 16$ excitatory cells with relatively strong cortical-cortical connection. For this small N, the network is strongly fluctuation-driven. The dynamics of this excitatory network exhibits bistability with a sharp transition as the average input conductance G_{input} is increased. Fig. 3 shows the bifurcation diagram for the firing rate m as a function of G_{input}. The theoretical prediction of the kinetic theory is compared with those of numerical simulation. The agreement is again extremely good, even for such a small number ($N = 16$) of neurons — with the small discrepancy due to the $\sigma \to 0$ asymptotics, and not to small N.

In addition to accuracy, the kinetic representation [Eqs. (10)] is far more efficient computationally than the full I&F network. The reduction is two-fold: 1) the pdf representation yields a great computation savings by eliminating the need of running either very long times or many ensembles of the same I&F network to reduce the statistical error in computing firing rates; 2) The reduction from the $(2+1)$-D systems (Eq. (4)) to the $(1+1)$-D PDE's (Eqs. (10)) provides really significant savings. For example, to achieve a rate computation within 1% accuracy for a network of 100 neurons, a reduction of 3-4 orders of magnitude in computation work can be easily obtained.

Next, and for the remainder of this section, we turn to a realistic CG cell containing the order of 200 neurons – with equal portion of simple and complex cells, of which 75% are excitatory and 25% inhibitory. Figure 4 shows theoretical bifurcation diagrams (m vs G_{input}) for two excitatory CG cells, one simple and one complex as predicted by our kinetic theory (The large-N, mean-driven limit, as well as the finite $N = 75$ case which captures the effects of fluctuations, are shown). Note the complicated bistable, hysteretic

structure of the large-N limit, as the simple and complex neuronal types jump between their respective lower and upper branches, inducing consequent changes in the firing rates of the other type. More importantly, note that for the network of *this particular cortical connection strength*, in the small-N case, the fluctuations are so strong, smoothing the firing curve so much so that there is no bifurcation/hysteresis.

Figure 5 shows bifurcation diagrams (firing rate m vs. G_{input}) for several values of cortico-cortical excitation strength S_{ee}^{cmplx} for complex neurons. These response diagrams compare the predictions of our kinetic theory (in the small-σ limit) with those computed by numerical simulations, with good qualitative agreement — for one CG cell containing both excitatory and inhibitory neurons of both simple and complex type. Figure 5a shows the theoretical results for excitatory neurons, one simple and one complex — while Fig 5b shows the same results computed by simulation. As S_{ee}^{cmplx} is increased, these response curves change from no bistability/hysteresis, through critical response, to bistability/hysteresis at strong S_{ee}^{cmplx}.

4 Discussion

These results begin to suggest that, depending on cortical connection strength, complex cells which are well selective for orientation may be the result of "upper branch" or "near-transition" behavior. Here, we describe some further evidence in this direction — from "ring models."

We begin from our large-scale I&F model of input layer $4C\alpha$ [6, 7, 5], and use it to introduce a family of idealized I&F "ring models", indexed by the radius of the ring away from a pinwheel. These I&F networks consist of 75% (25%) excitatory (inhibitory) neurons. One half of the cells (the simple cells) are driven by the LGN with weak cortico-cortical excitation, in contrast to the other half (the complex cells), which receive no LGN drive, but have stronger cortico-cortical excitation. This simple/complex architecture is shown schematically in Fig. 1a. The ring models can be thought of as idealizations of this large scale network, with the I&F neurons restricted to reside on a circle centered upon an orientation pinwheel center (See the white circle in Fig 1b.) [19, 15, 14] In the models, the neighboring cortico-cortical coupling strengths are taken to decay as a Gaussian, falling off with distance

between the neurons — cortical distance in the case of the large scale model and angular distance in the ring models. The radius of the ring is used to convert the cortical coupling lengths of neurons in the large scale model to coupling lengths in the angle γ along the ring — with broad coupling lengths in γ for rings of small radii (whose neurons reside close to the pinwheel center), and narrow couplings in γ for rings of large radii (whose neurons reside far from the pinwheel center).

We drive these models with drifting gratings, with angle of orientation θ. Figure 6 shows orientation tuning curves (firing rate $m(\theta)$ with the angle θ the orientation of the drifting grating) for simple (dashed) and complex (solid) cells in two ring models — one with weak fluctuations (Fig. 6a), and the other with stronger fluctuations (Fig. 6b) achieved by removing the slow NMDA excitatory synapses from the network while keeping the cortical-cortical coupling strength the same. Note the tuning curves shown in Figure 6a display the characteristics of a mean driven, high conductance state with weak fluctuations — characteristics identified through use of the kinetic representations: abnormally high firing rates of the complex cell, together with the very low firing rates of the simple cell; very sharp transitions (in θ) in the firing rate of the complex cell; and a strong synchrony in the firing patterns of the complex cells (as shown in the raster plot inset). On the other hand, the tuning curves of Figure 6b display the characteristics of a fluctuation driven state: more reasonable firing rates; a more gradual behavior as a function of θ; and the lack of synchrony in the firing patterns of the complex cells (again shown in the raster plot inset).

Figure 7 shows results for two ring models [one of small radius (Figs. 7a & 7d), whose neurons are close to the pinwheel center, and one of larger radius (Figs. 7b & 7e), whose neurons are far from the pinwheel center]; together with results for the full large-scale network (Figs. 7c & 7f). Figs. 7a,7b & 7c show orientation tuning curves (firing rate $m(\theta)$; while Figs. 7d,7e &7f show bifurcation diagrams (firing rate m vs. the strength of the conductance drive). The samples shown are complex cells. In the bifurcation diagrams, heavy bold curves show behavior during "switch-up" of the driving strength, while regular curves depict responses to "switch-down". The dashed lines in Figs. 7a & 7b depict the results from the kinetic theory extended to the ring model with excitatory, inhibitory, simple and complex neurons. In this

extension of the kinetic theory, the coarse-grained cells are coupled according to Eq. (11), with the angular variable θ replacing the spatial variable $\mathbf{x}$ as the labeling of the CG cells in the ring model.

Note that **(i)** Each of these three networks appears to be operating in a fluctuation driven regime, based upon the characteristics described above, and identified through kinetic theory and confirmed by I& F dynamics. **(ii)** For the ring of small radius (Figs. 7a & 7d), the firing rates rise rather gradually with increasing driving strength. **(iii)** The opposite is true for the ring of large radius — which has a much steeper dependence of firing rate on driving strength. This indicates that this well tuned complex cell is operating at, or near, an upper branch. However, while steep, it does not yet display hysteresis nor bistability.

In all cases shown (ring models and the full large scale network), there is no hysteresis nor bistability — although the complex cell in the large ring shows steep dependence upon driving strength — almost as if "pre-hysteretic." This behavior, together with that of the orientation tuning curves in this case (Fig. 7b), provides a strong indication that those complex cells which are quite selective for orientation might result from upper branch behavior which is at least pre-hysteretic. We [5] have yet to construct a large-scale network which operates realistically in this regime – primarily because, as the regime is approached, instabilities in the network appear and cause synchronization of the neurons which is reminiscent of the mean-driven state with small fluctuations.

The new kinetic theory described here clearly provides theoretical insight into cortical mechanisms in fluctuation dominated systems. It also provides an efficient computational method for numerical studies of very large scale neuronal networks. More detailed study, using kinetic theory, of large scale networks of simple and complex cells will be published elsewhere.

References

[1] Anderson, J, Lampl, I, Gillespie, D, & Ferster, D. (2000) *Science* **290**, 1968–1972.

[2] Shelley, M & McLaughlin, D. (2002) *J. Comput. Neurosci.* **12**, 97–122.

[3] Fourcaud, N & Brunel, N. (2002) *Neural Comp.* **14**, 2057–2110.

[4] Hubel, D & Wiesel, T. (1962) *J. Physiol. (Lond)* **160**, 106–154.

[5] Tao, L, Shelley, M, McLaughlin, D, & Shapley, R. (2004) *Proc. Natl. Acad. Sci. USA* **101**, 366–371.

[6] McLaughlin, D, Shapley, R, Shelley, M, & Wielaard, J. (2000) *Proc. Natl. Acad. Sci. USA* **97**, 8087–8092.

[7] Wielaard, J, Shelley, M, Shapley, R, & McLaughlin, D. (2001) *J. Neurosci.* **21**.

[8] Knight, B. (1972) *J. Gen. Physiol.* **59**, 734–766.

[9] Wilbur, W & Rinzel, J. (1983) *J. Theor. Biol.* **105**, 345–368.

[10] Abbott, L & van Vreeswijk, C. (1993) *Phys. Rev. E* **48**, 1483–1490.

[11] Brunel, N & Hakim, V. (1999) *Neural Comp.* **11**, 1621–1671.

[12] Gerstner, W. (2000) *Neural Comp.* **12**, 43–89.

[13] Omurtag, A, Knight, B, & Sirovich, L. (2000) *J. Comp. Neurosci.* **8**, 51–63.

[14] Omurtag, A, Kaplan, E, Knight, B, & Sirovich, L. (2000) *Network* **11**, 247–60.

[15] Nykamp, D & Tranchina, D. (2000) *J. Comp. Neurosci.* **8**, 19–50.

[16] Nykamp, D & Tranchina, D. (2001) *Neural Comp.* **13**, 511–546.

[17] Cinlar, E. (1972) ed. Lewis, P. (Wiley, New York, NY).

[18] Treves, A. (1993) *Network* **4**, 259–284.

[19] Somers, D, Nelson, S, & Sur, M. (1995) *J. Neurosci.* **15**, 5448–5465.

[20] Blasdel, G. (1992) *J. Neurosci.* **12**, 3115–3138.

[21] Blasdel, G. (1992) *J. Neurosci.* **12**, 3139–3161.

5 Figure Captions

Figure 1: a) *A schematic of the network*, indicating the mechanisms by which simple and complex cells are created — with simple cells by strong LGN input, strong cortical inhibition, together with phase randomization (not shown); and complex cells by weak LGN input and stronger cortical excitation. b) Optical image of the map of orientation preference, for $\simeq 1mm^2$ of layer 2-3 of macaque V1 — containing 4 pinwheel centers [20, 21]. The cells on the circle are described by our ring model (see Discussion). c) A schematic of one CG cell located, for example, on a small section of a ring.

Figure 2: *Comparison of predictions of the kinetic theory* (Eqs. (10)) *with those of full numerical simulation of the I&F network* for a single CG cell with $N = 75$ neurons, all excitatory, simple type ($\sigma = 5ms$ and $\tau = 20ms, S = 0.05, f = 0.01$). a) and b): $\rho^{(v)}(v)$ and $\rho^{(g)}(g)$, respectively — solid curves theoretical and circles simulations, and c) the average population firing rates per neuron m as a function of the average input conductance G_{input} for $\sigma = 5ms$ (dashed) and $\sigma = 0ms$ (dash-dotted). Note the failure of the mean-driven theory ($N \to \infty, f \to 0$) (dotted line), which neglects fluctuations.

Figure 3: *Bifurcation diagrams* for the firing rate m vs. average input conductance G_{input} which compare numerical simulation results with the prediction of the kinetic theory (Eq. (10) in the small σ-limit) — for a CG cell containing a small number ($N = 16$) of excitatory neurons with all-to-all connections ($\sigma = 5ms$, $S = 0.45, \tau_{ref} = 3ms$). Theory (thick dashed line) shows lower and upper branches of bistability, with a sharp transition from A to B. Simulation results are obtained by slowly "ramping" G_{input} — first up, then down. Arrows indicate the results of the simulations with respect to ramping G_{input} up and down. The inset zooms into the transition region, for different realizations of input Poisson spikes.

Figure 4: *Bifurcation diagrams* (excitatory firing rate m vs. average input conductance G_{input}) predicted by the kinetic theory — for a realistic CG cell, 1/2 of which are simple and 1/2 of which are complex, and 3/4 (1/4) of which are excitatory (inhibitory). The large figure displays the large N limit, and the inset is the finite $N = 75$ fluctuation driven result; and in each case, firing curves are shown for both simple (dotted or dash-dotted) and complex excitatory (dash or solid) cells. Note the complicated structure

of the mean-driven ($N \to \infty$) case which results from an interplay between the bifurcations of the simple and complex cells. In more detail: At point A — simple cells reaches its firing threshold in terms of G_{inp} and begin to fire. With increasing G_{inp}, the firing curve follows $A \to D \to B$. At the same time, due to the increasing input from the simple cells, the complex cells reach firing threshold at point B' in terms of G_{inp} and abruptly jump from zero firing rate to point C'. Due to this jump, the firing rate of simple cells jumps from B to C. If G_{inp} is decreased, the firing curve of complex cells follows $C' \to D'$ and shuts off at D' while the simple cells follow the corresponding firing curve, starting from C and revisiting D. With G_{inp} further decreasing, the simple cells trace the firing curve AD backward to point A and, then, shuts off. The complex cells exhibit a hysteretic loop $D'B'C'D'$. Associated with this is the hysteretic loop $DBCD$ for the simple cells. Note that fluctuations smooth the bifurcations, as clearly shown in the inset for the network of this particular cortical-cortical connection strength.

Figure 5: *Bifurcation diagrams* (excitatory firing rate m vs. average input conductance G_{input}) — for a realistic CG cell containing 400 I&F neurons, 1/2 of which are simple and 1/2 of which are complex, and 3/4 (1/4) of which are excitatory (inhibitory) with random connections to only 1/4 of other cells. a) Prediction of our kinetic theory; b) results from numerical simulation of the I&F network. The figures show results for simple (light lines) and complex (heavy lines) excitatory neurons, for increasing values of the coupling strengths of cortico-cortical excitation for complex type. The theoretical results in a) show a steepening of the curves as coupling strength is increased — from monotonic, through critical, to bistable. The corresponding simulation results b) show the same behavior with the bistability being manifested in the hysteresis.

Figure 6: *Orientation tuning curves* for a ring model containing excitatory and inhibitory neurons of both simple (dashed) and complex (solid) type — computed from numerical simulations of an integrate and fire network. a) A mean driven state with negligible fluctuations. Note the characteristics of a mean-driven, high conductance state: abnormally high firing rates in the complex cell, together with the very low firing rates of the simple cell; the sharp transition in the firing rate of the complex cell as a function of θ; and the strong synchrony in the firing patterns of the complex cells (as

shown in the raster plot inset). b) A fluctuation-driven state. Note the more reasonable firing rates; their more gradual behavior as a function of θ; and the lack of synchrony in the firing patterns of the complex cells (again shown in the raster plot inset).

Figure 7: *Comparison of the firing rate behavior under drifting grating stimuli of three neuronal networks* — two ring models and our [5] large scale I&F $1mm^2$ model. Each of the models contains 75% (25%) excitatory (inhibitory) neurons, and simple and complex cells. Figures a,b & c show orientation tuning curves (firing rate $m(\theta)$, where θ denotes the orientation of the drifting grating) comparing the results of the full I&F networks (solid line) with those the kinetic theory (dashed line); while figures d,e & f show bifurcation diagrams ($m(\theta)$ vs. the driving strength). In the bifurcation diagrams, heavy bold curves show behavior during "switch-up" of the driving strength, while regular curves depict responses to "switch-down". **Figures a & d:** A ring model of small radius (with neurons near the pinwheel center); **Figures b & e:** A ring model of large radius (far from pinwheel center); **Figures c & f:** Neurons from the large-scale model which are far from any pinwheel center.

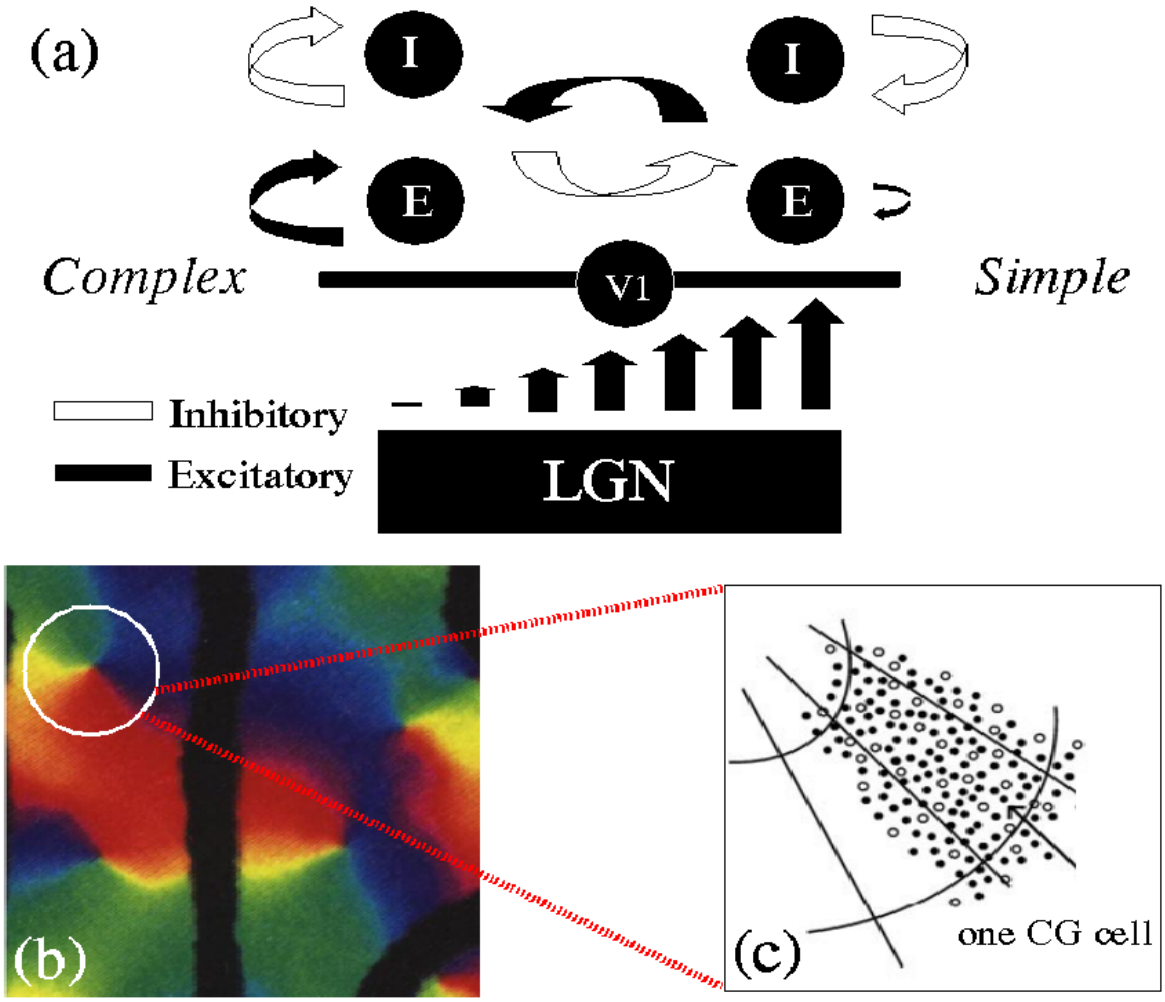

Figure 1: a) *A schematic of the network*, indicating the mechanisms by which simple and complex cells are created – with simple cells by strong LGN input, strong cortical inhibition, together with phase randomization (not shown); and complex cells by weak LGN input and stronger cortical excitation. b) Optical image of the map of orientation preference, for $\simeq 1mm^2$ of layer 2-3 of macaque V1 – containing 4 pinwheel centers [20, 21]. The cells on the circle are described by our ring model (see Discussion). c) A schematic of one CG cell located, for example, on a small section of a ring.

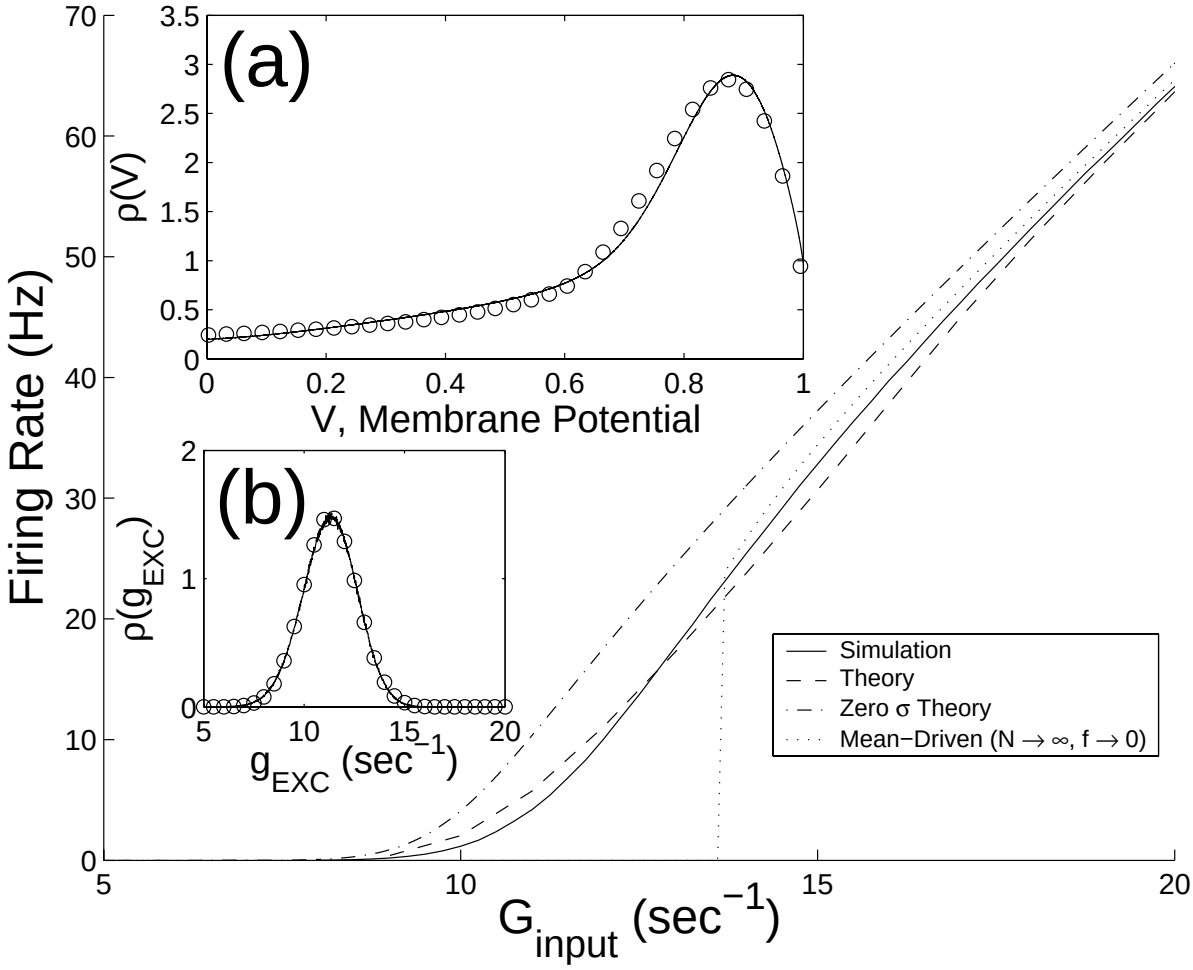

Figure 2: *Comparison of predictions of the kinetic theory* (Eqs. (10)) *with those of full numerical simulation of the I&F network* for a single CG cell with $N = 75$ neurons, all excitatory, simple type ($\sigma = 5ms$ and $\tau = 20ms, S = 0.05, f = 0.01$). a) and b): $\rho^{(v)}(v)$ and $\rho^{(g)}(g)$, respectively — solid curves theoretical and circles simulations, and c) the average population firing rates per neuron m as a function of the average input conductance G_{input} for $\sigma = 5ms$ (dashed) and $\sigma = 0ms$ (dash-dotted). Note the failure of the mean-driven theory ($N \to \infty, f \to 0$) (dotted line), which neglects fluctuations.

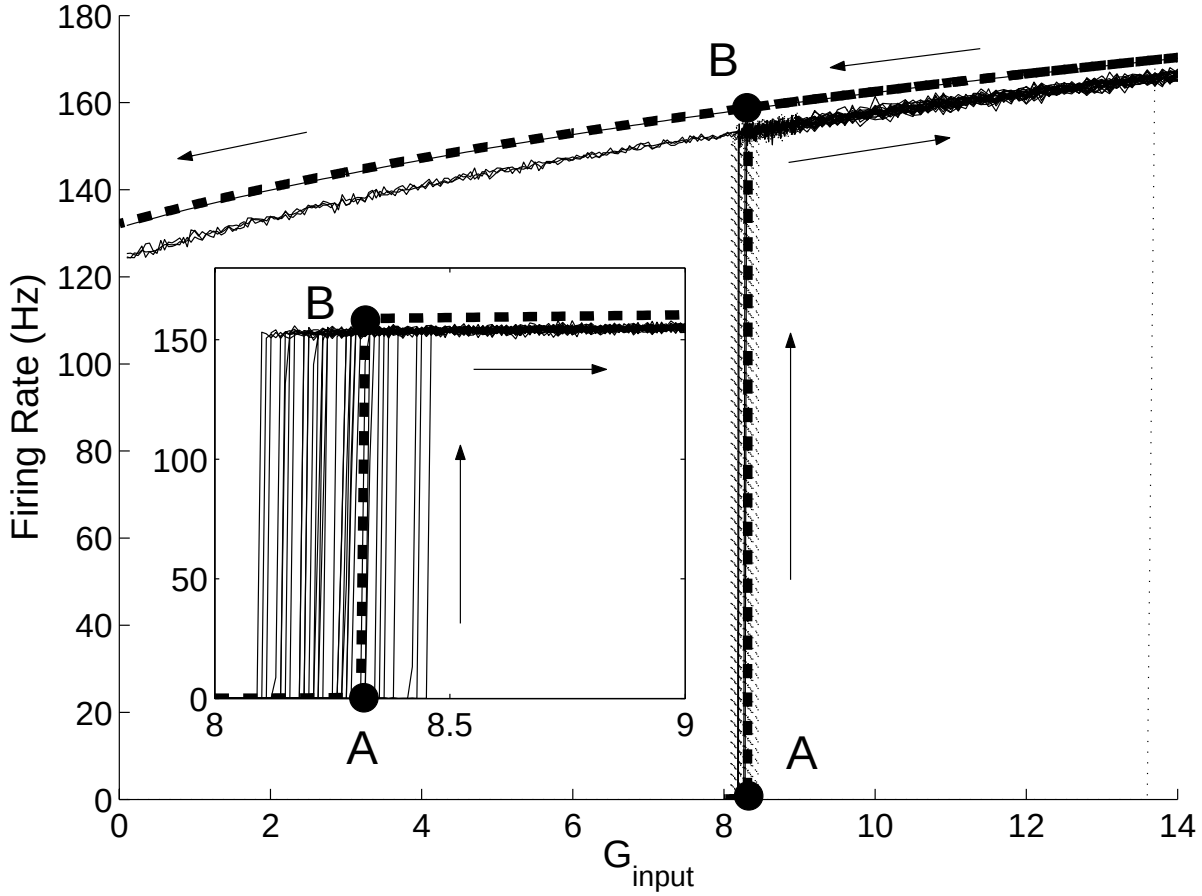

Figure 3: *Bifurcation diagrams* for the firing rate m vs average input conductance G_{input} which compare numerical simulation results with the prediction of the kinetic theory (Eq. (10) in the small σ-limit) — for a CG cell containing a small number ($N = 16$) of excitatory neurons with all-to-all connections ($\sigma = 5ms$, $S = 0.45, \tau_{ref} = 3ms$). Theory (thick dashed line) shows lower and upper branches of bistability, with a sharp transition from A to B. Simulation results are obtained by slowly "ramping" G_{input} — first up, then down. Arrows indicate the results of the simulations with respect to ramping G_{input} up and down. The inset zooms into the transition region, for different realizations of input Poisson spikes.

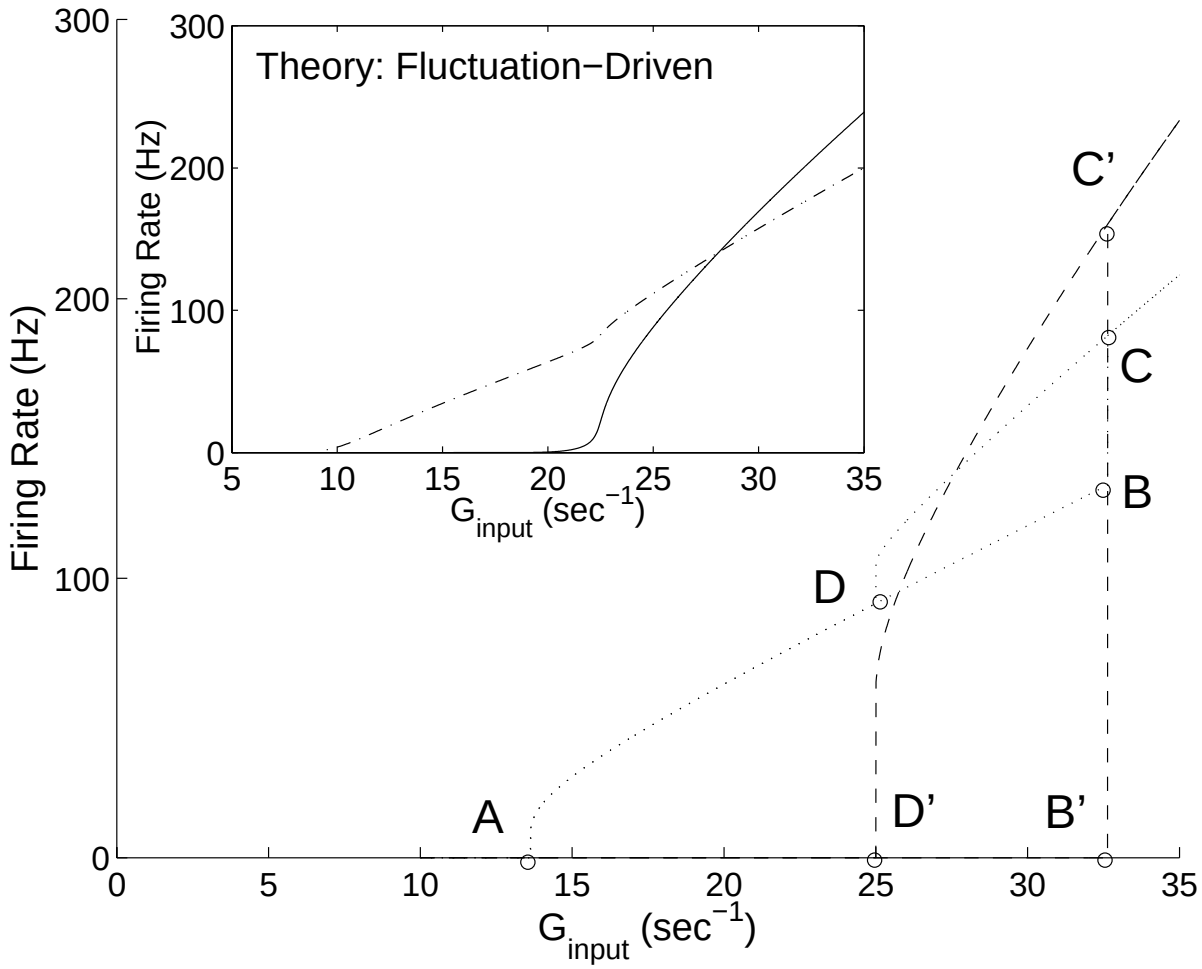

Figure 4: *Bifurcation diagrams* (excitatory firing rate m vs average input conductance G_{input}) predicted by the kinetic theory — for a realistic CG cell, 1/2 of which are simple and 1/2 of which are complex, and 3/4 (1/4) of which are excitatory (inhibitory). The large figure displays the large N limit, and the inset is the finite $N = 75$ fluctuation driven result; and in each case, both simple and complex excitatory firing curves are shown. Note the complicated structure of the mean-driven ($N \to \infty$) case which results from an interplay between the bifurcations of the simple and complex cells. In more detail: At point A — simple cells reaches its firing threshold in terms of G_{inp} and begin to fire. With increasing G_{inp}, the firing curve follows $A \to D \to B$. At the same time, due to the increasing input from the simple cells, the complex cells reach firing threshold at point B' in terms of G_{inp} and abruptly jump from zero firing rate to point C'. Due to this jump, the firing rate of simple cells jumps from B to C. If G_{inp} is decreased, the firing curve of complex cells follows $C' \to D'$ and shuts off at D' while the simple cells follow the corresponding firing curve, starting from C and revisiting D. With G_{inp} further decreasing, the simple cells trace the firing curve AD backward to point A and, then, shuts off. The complex cells exhibit a hysteretic loop $D'B'C'D'$. Associated with this is the hysteretic loop $DBCD$ for the simple cells. Note that fluctuations smooth the bifurcations, as clearly shown in the inset for the network of this particular cortical-cortical connection strength.

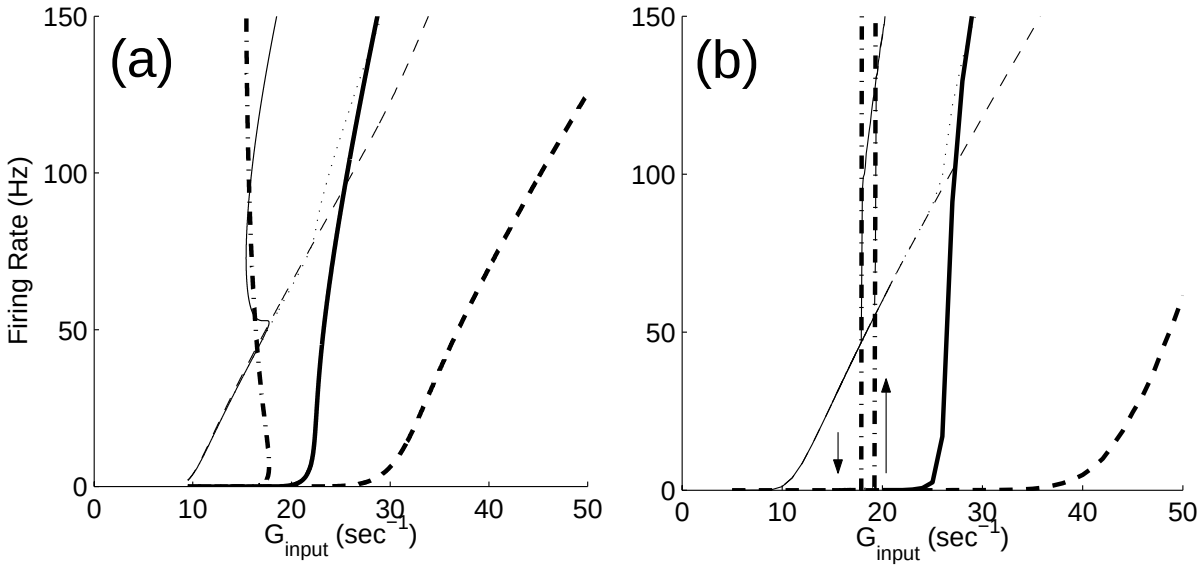

Figure 5: *Bifurcation diagrams* (excitatory firing rate m vs average input conductance G_{input}) – for a realistic CG cell containing 400 I&F neurons, 1/2 of which are simple and 1/2 of which are complex, and 3/4 (1/4) of which are excitatory (inhibitory) with random connections to only 1/4 of other cells. a) Prediction of our kinetic theory; b) results from numerical simulation of the I&F network. The figures show results for simple (light lines) and complex (heavy lines) excitatory neurons, for increasing values of the coupling strengths of cortico-cortical excitation for complex type. The theoretical results in a) show a steepening of the curves as coupling strength is increased – from monotonic, through critical, to bistable. The corresponding simulation results b) show the same behavior with the bistability being manifested in the hysteresis.

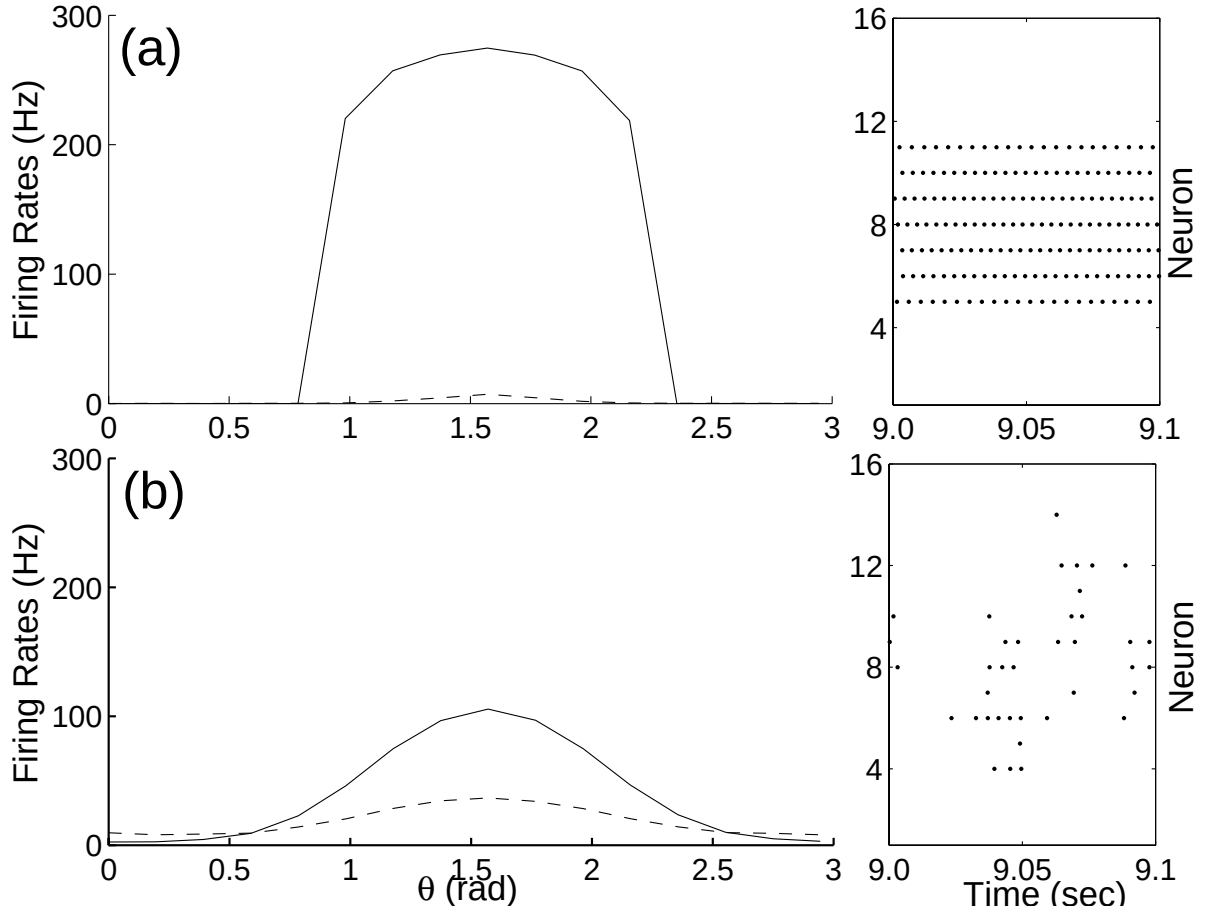

Figure 6: *Orientation tuning curves* for a ring model containing excitatory and inhibitory neurons of both simple (dashed) and complex (solid) type – computed from numerical simulations of an integrate and fire network. a) A mean driven state with negligible fluctuations which results from strong cortico-cortical excitation. Note the characteristics of a mean driven, high conductance state: abnormally high firing rates in the complex cell, together with the very low firing rates of the simple cell; the sharp transition in the firing rate of the complex cell as a function of θ; and the strong synchrony in the firing patterns of the complex cells (as shown in the raster plot insert). b) A fluctuation driven state which results from less cortico-cortical excitation. Note the more reasonable firing rates; their more gradual behavior as a function of θ; and the lack of synchrony in the firing patterns of the complex cells (again shown in the raster plot inset).

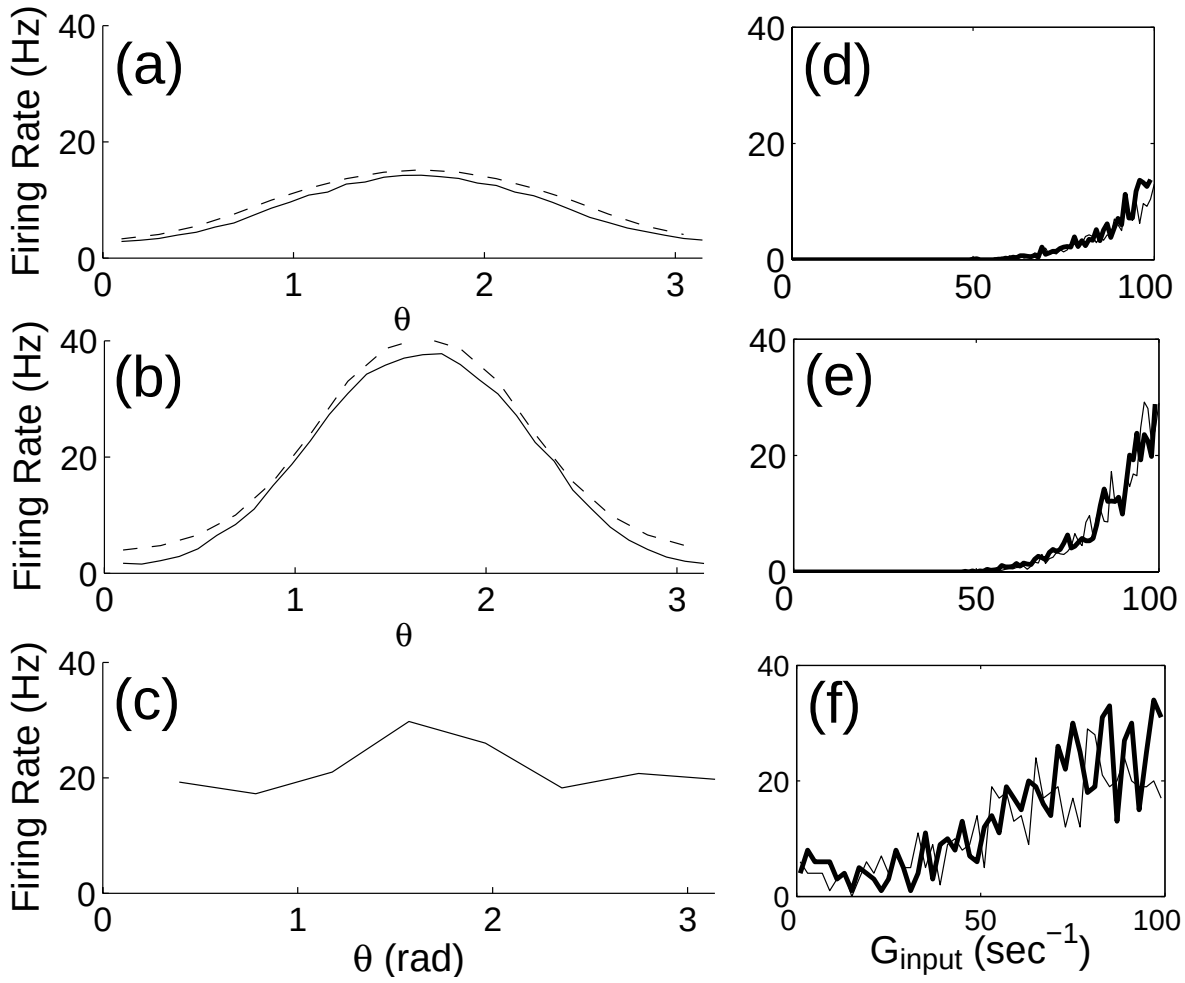

Figure 7: *Comparison of the firing rate behavior under drifting grating stimuli of three integrate and fire neuronal networks* – two ring models and our [5] large scale I& F $1mm^2$ model. Each of the models contains 75% (25%) excitatory (inhibitory) neurons, and simple and complex cells. Figures a,b & c show orientation tuning curves (firing rate $m(\theta)$, where θ denotes the orientation of the drifting grating) comparing the results of the full I&F networks (solid line) with those the kinetic theory (dashed line); while figures d,e & f show bifurcation diagrams ($m(\theta)$ vs the driving strength). In the bifurcation diagrams, heavy bold curves show behavior during "switch-up" of the driving strength, while regular curves depict responses to "switch-down". **Figures a & d:** A ring model of small radius (with neurons near the pinwheel center); **Figures b & e:** A ring model of large radius (far from pinwheel center); **Figures c & f:** Neurons from the large-scale model which are far from any pinwheel center.